

A transportable strontium optical lattice clock

N. Poli,¹ M. Schioppo,^{1,*} S. Vogt,² St. Falke,^{2,†} U. Sterr,² Ch. Lisdat,² and G. M. Tino¹

¹*Dipartimento di Fisica e Astronomia and LENS,*

Università di Firenze and INFN Sezione di Firenze, Via Sansone 1, 50019 Sesto Fiorentino, Italy

²*Physikalisch-Technische Bundesanstalt, Bundesallee 100, 38116 Braunschweig, Germany*

(Dated: January 26, 2022)

We report on a transportable optical clock, based on laser-cooled strontium atoms trapped in an optical lattice. The experimental apparatus is composed of a compact source of ultra-cold strontium atoms including a compact cooling laser set-up and a transportable ultra-stable laser for interrogating the optical clock transition. The whole setup (excluding electronics) fits within a volume of less than 2 m³. The high degree of operation reliability of both systems allowed the spectroscopy of the clock transition to be performed with 10 Hz resolution. We estimate an uncertainty of the clock of 7×10^{-15} .

I. INTRODUCTION

As the development of optical clocks is currently pursued in many laboratories worldwide [1–4], a broad range of applications is taking shape with optical clocks on ground and in space employed for high precision tests of fundamental physics [5, 6], chronometric levelling-based geodesy [7], improved RF standards for navigation [8] and observations of cosmic radio sources with very-long baseline interferometry (VLBI) [9]. For all these purposes today’s complex and bulky optical-clock experimental setups need to be re-engineered into more compact and power efficient systems, ensuring at the same time a high stability and accuracy, but also high operation reliability in critical environments [10], such as application in the field or even satellites.

A first step in the engineering challenge leading to space based optical clocks is to demonstrate transportable clocks. These are interesting because frequency comparisons of today’s best optical clocks cannot be done through satellite links and tests with optical fiber links require dedicated equipment [11–13]. A frequency transfer standard will allow for comparing clocks at the accuracy level provided by the transportable clock [14].

In this paper we present the realization of a transportable strontium optical clock, based on the integration of two subsystems, a compact atomic source including a compact cooling and trapping laser set-up, and a transportable clock laser, providing the laser-cooled sample of strontium atoms and the ultra-stable radiation source for interrogating the clock transition, respectively. The clock laser, transported by van from PTB in Braunschweig to LENS in Florence was employed to perform high resolution spectroscopy of the clock transition 1S_0 - 3P_0 of ^{88}Sr in Lamb-Dicke regime and to characterize systematic frequency shifts of the optical transition.

In the following are presented in detail novel design solutions employed for each subsystem that allowed us to reduce size, weight and power consumption with respect to a traditional laser cooling apparatus.

II. THE TRANSPORTABLE CLOCK SETUP

A. Compact system for cooling and trapping strontium atoms

The compact laser-cooling strontium source mainly consists of the following modules: the cooling laser sources, a frequency distribution breadboard and a vacuum system. The three modules are connected through optical fibers and mounted directly on a 120 cm \times 90 cm breadboard. The control electronics is hosted under the main breadboard in a 19” rack (size 60 cm \times 60 cm \times 180 cm).

Cooling and trapping of strontium atoms is performed through a two-stage magneto-optical-trap (MOT) on the dipole allowed 1S_0 - 1P_1 transition and on the intercombination line 1S_0 - 3P_1 , respectively (see Fig. 1). All the employed lasers are based on semiconductor diodes [15, 16]. The laser set is composed of a frequency doubled 300 mW 461 nm laser, a 50 mW 689 nm laser, a 420 mW 813 nm (master + tapered amplifier) laser and two \sim 20 mW 679 nm and

*Present address: National Institute of Standards and Technology, Time and Frequency Division, MS 847, Boulder, CO 80305, USA

†Present address: TOPTICA Photonics AG, Lochhamer Schlag 19, 82166 Graefelfing (Munich), Germany

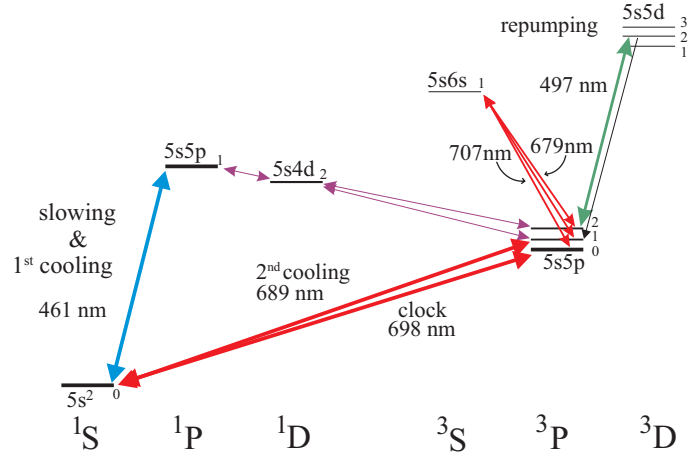


FIG. 1: Energy levels and relevant optical transition for neutral Sr. The number near the level is the total angular momentum J .

707 nm repumper lasers. These sources are used for the two-stage laser-cooling and subsequent optical trapping in a one-dimensional (1D) lattice at the magic wavelength [17].

All the optical beams for the first laser-cooling stage at 461 nm are produced in a compact module (size $30 \text{ cm} \times 40 \text{ cm} \times 8 \text{ cm}$). The module contains ultra-stable mountings for mirrors, polarization cubes, plates, lenses and acousto-optic-modulators (AOMs) to which the 461 nm radiation is delivered by fibre [18].

In order to reduce the number of beam shaping optical elements used in the breadboard while maintaining a high diffraction efficiency on AOMs, an input beam $1/e^2$ diameter has been set to 0.5 mm. As a result we obtain high diffraction efficiency on AOMs ($>80\%$ in single pass configuration) without the use of any additional telescope, while still keeping the possibility of resolving the diffraction orders at short distances. Moreover with this choice a coupling efficiency into optical fibers of about 65 % is achieved. Then, the overall efficiency of a typical $\sim 25 \text{ cm}$ long optical path inside the breadboard, including the AOM diffraction efficiency (in single-pass configuration) and the coupling efficiency into the output fiber, is typically $\sim 50\%$. The frequency detunings from the 1S_0 - 1P_1 resonance for Zeeman slower and MOT beams, of -320 MHz and -40 MHz respectively, are obtained by using two AOMs in single-pass configuration, driven at 170 MHz ($-$ order) and 110 MHz ($+$ order), respectively. All output beams can also be completely shut off by fast and compact mechanical shutters. A beam for frequency stabilization of the first stage cooling light is obtained from a double-pass configuration through an AOM driven at 75 MHz and sent to the atomic beam used to load the MOT (see Fig. 2). In order to extract an error signal from spectroscopy on the cooling transition, the driving RF signal is also frequency modulated at $\sim 10 \text{ kHz}$ with a peak to peak deviation of $\sim 10 \text{ MHz}$. A low power ($\sim 1 \text{ mW}$) resonant beam for absorption imaging is generated in a similar double pass configuration. For both double-pass AOMs a cat's-eye configuration has been realized by focusing the optical beam on the retro-reflecting mirror with a lens at distance $f = 60 \text{ mm}$ from AOM and retro-reflection mirror.

The atomic sample is trapped in a vacuum system (size $1200 \text{ cm} \times 40 \text{ cm} \times 36 \text{ cm}$), see Fig. 2) consisting of the oven region, where a collimated Sr atomic beam is produced, a Zeeman slower and the science region where the Sr atoms are subsequently Zeeman slowed, trapped in a two-stage MOT and eventually transferred in a 1D vertical optical lattice for clock spectroscopy. The oven region is pumped by a 40 l/s ion pump (pressure during operation $\sim 10^{-6} \text{ Pa}$), the science region is evacuated by a 55 l/s ion pump and a titanium sublimation pump (pressure $\sim 10^{-7} \text{ Pa}$). A differential pumping tube (internal diameter 5 mm , length 7.5 cm) ensures to maintain the pressure difference between the two regions.

In the oven region, atoms are sublimated by a compact and efficient dispenser [19] based on a heater placed in vacuum, providing an atomic flux intensity of $1.7 \times 10^{13} \text{ s}^{-1} \text{ sr}^{-1}$ (^{88}Sr atoms) at the oven temperature of 380°C with a total power consumption of 26 W . The atomic beam is collimated by a nozzle of about 120 capillaries (internal diameter $200 \mu\text{m}$, length 8 mm). The high collimation ($\sim 40 \text{ mrad}$) and flux allow the laser stabilization to be performed with high signal-to-noise employing a simple transverse fluorescence spectroscopy on the atomic beam in the oven chamber (see Fig. 2). The atomic beam propagates along a 23 cm long tube externally wrapped with coils for Zeeman slowing. The magnetic field shape for Zeeman slowing has been designed to smoothly match the off-axis component of the MOT coils' field (see Fig. 4) [18]. The first part of the Zeeman slower (before the inversion of the field given by the MOT coils) has a length of 18 cm and it operates with a power consumption of 17 W .

The decelerated atomic beam is trapped in a MOT at the center of a science cell with eight CF40 and sixteen CF16

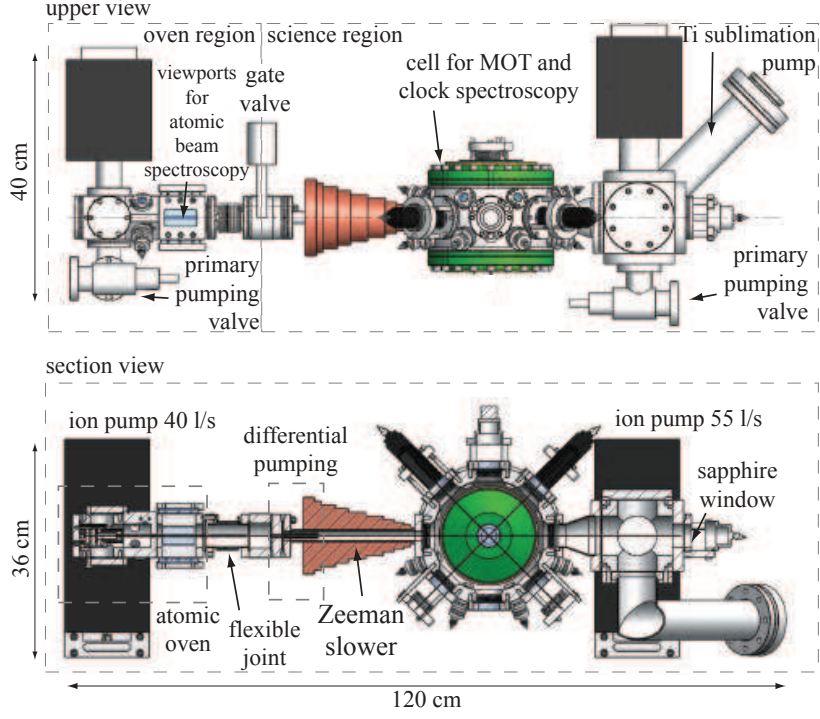


FIG. 2: Technical drawing of the vacuum system (upper view and section side view) showing the main part of the system (the oven region, on the left and the science region, on the right.).

optical windows. Two custom CF150 flanges host the pair of coils (in anti-Helmholtz configuration as needed for MOT operation) outside the MOT chamber 2.6 cm away from the atoms. In this configuration a magnetic field gradient of ~ 500 mT/m is obtained with a total power consumption of ~ 60 W. With these levels of power consumption for oven, Zeeman slower and MOT coils we could avoid the complication of water cooling, with a typical chamber temperature of 318 K.

To make the alignment of the MOT beams long-term stable, the cooling beams at 461 nm and 689 nm are delivered by three dichroic fiber-coupled beam expanders fastened to the science cell. A system of setting screws and counter screws allows fine alignment and locking of the MOT beams. Similarly, the MOT beam retroreflectors, repumping, imaging and clock spectroscopy output-couplers are fastened onto the science cell. The alignment of the MOT beams has been maintained for more than one year without any further adjustment.

B. Transportable clock laser

The main clock laser breadboard is based on two diode lasers in a master-slave setup. The master is a filter stabilized extended cavity laser with resonator length 10 cm [20]. About 0.5 mW of the master-laser power is used to injection lock the slave laser. The breadboard has a total size of $60 \text{ cm} \times 45 \text{ cm} \times 10 \text{ cm}$, its design is similar to frequency distribution breadboard presented in the previous section. A 200 MHz AOM in double-pass configuration is used to bridge the frequency gap between the optical resonator with free spectral range of 1.5 GHz and the frequency of the clock transition. This AOM is used to scan the frequency of the laser and also to enable frequency feedback when the laser is locked to the clock transition. Two output ports for clock spectroscopy and for counting of the laser frequency provide a maximum optical power of about 2 mW each. Both ports are provided with AOMs for switching which can also be used to stabilize the optical path length of the fibers. The interferometric setup for this stabilization is included on the breadboard [21]. The laser was locked to a transportable high finesse cavity whose transportability had already been demonstrated within the SOC project [22].

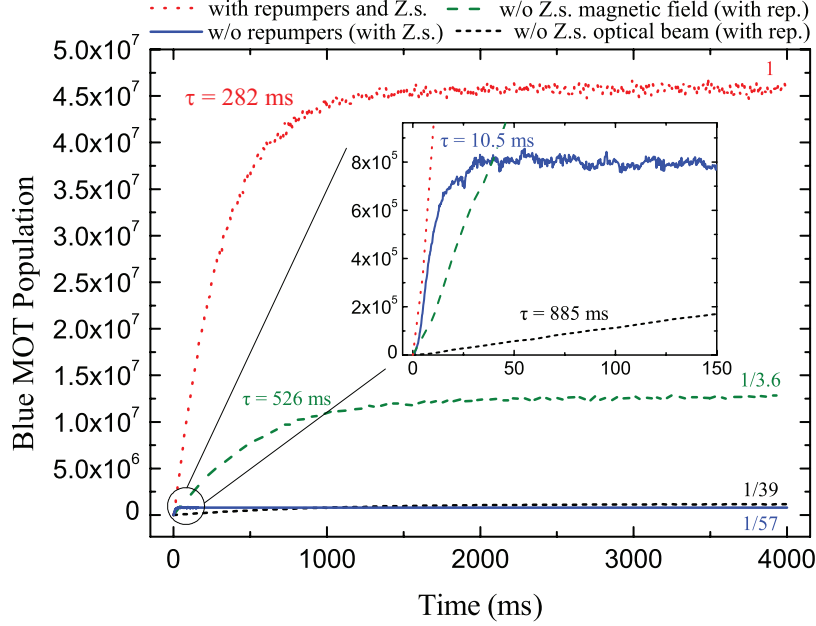


FIG. 3: Comparison among blue MOT loading curves and final blue MOT population obtained with repumpers and Zeeman slower beam (red dash), without Zeeman slower magnetic field (green dash), without repumpers (blue line) and without Zeeman slower beam (black dash).

III. EXPERIMENTAL RESULTS

A. Cooling and trapping

In order to develop a more compact and low power consumption experimental system for the production of ultra-cold strontium atoms, several design solutions have been adopted, together with an optimization of the efficiency of each cooling and trapping step. In order to slow down the atoms sublimating from the oven from 430 m/s to below 130 m/s, an optical beam at 461 nm, circularly polarized, is sent counter propagating to the atomic beam. The laser beam has an optical power of 30 mW, an initial $1/e^2$ radius of $r = 5$ mm, focused after 1 m to compensate the absorption of photons in the slowing process. Atoms are kept in resonance during the slowing by compensating the variation of Doppler shift with the proper Zeeman shift from the magnetic field provided by the Zeeman slower. The sample of cold ^{88}Sr atoms is produced through two laser-cooling stages. The first stage consists of a MOT operating on the $^1\text{S}_0 - ^1\text{P}_1$ transition at 461 nm. This so called blue MOT is realized by three pairs of counter-propagating optical beams, circularly polarized, detuned by $\delta_L = -2\pi \times 40$ MHz, with a saturation parameter for each beam of $s \sim 1$ and a magnetic field gradient of 500 mT/m. The blue MOT capture velocity is $v_c = \sqrt{2a_{\text{max}}r} \simeq 100$ m/s where $a_{\text{max}} = \frac{1}{M} \hbar k_L \frac{\Gamma}{2} \frac{s}{1+s}$ is the maximum acceleration exerted by cooling light, with $k_L = 2\pi/\lambda$ the wavevector of the photons at $\lambda = 461$ nm, $\Gamma = 2\pi \times 32$ MHz the natural linewidth of the $^1\text{S}_0 - ^1\text{P}_1$ transition and M the atomic mass of strontium 88. As expected we find that the Zeeman slower increases the loading rate of the MOT, resulting in a net increase of the blue MOT population by a factor of ~ 40 (see Fig. 3).

The $^1\text{S}_0 - ^1\text{P}_1$ transition used for the blue MOT is not perfectly closed due to the decay channel of the $5p\ ^1\text{P}_1$ state towards the $4d\ ^1\text{D}_2$ state, which has a lifetime of 0.5 ms [23]. Atoms in the latter state may decay to the ground state through the $5p\ ^3\text{P}_1$ within less than 1 ms or may decay to the metastable $5p\ ^3\text{P}_2$ state and be lost. In order to recycle the atoms stored in the metastable $5p\ ^3\text{P}_2$ state a 10 mW repumper laser at 707 nm is used to pump these atoms in the $6s\ ^3\text{S}_1$ state. An additional 10 mW laser at 679 nm is necessary to deplete the $^3\text{P}_0$ state since it is also coupled to the $6s\ ^3\text{S}_1$ state. The repumping laser beams are superimposed, expanded to 10 mm of diameter and sent to the blue MOT and retroreflected. The repumping increases the atom number in the blue MOT by a factor ~ 60 . We studied the loading dynamics of the blue MOT population N , given by $dN/dt = \phi_c - \Gamma_L N - \beta' N^2$, where ϕ_c is the effective loading rate of atoms in the MOT, Γ_L is the linear loss rate (mainly due to background collisions when repumpers are operating) and β' is the coefficient for two-body collisional loss [24]. The previous equation with the initial condition $N(t=0) = 0$ has the standard solution $N(t) = N_{st}(1 - \exp(-t/\tau))/(1 - \xi \exp(-t/\tau))$ where N_{st} is the stationary number of trapped atoms, τ is the effective trap loading time and ξ is the collisional loss fraction

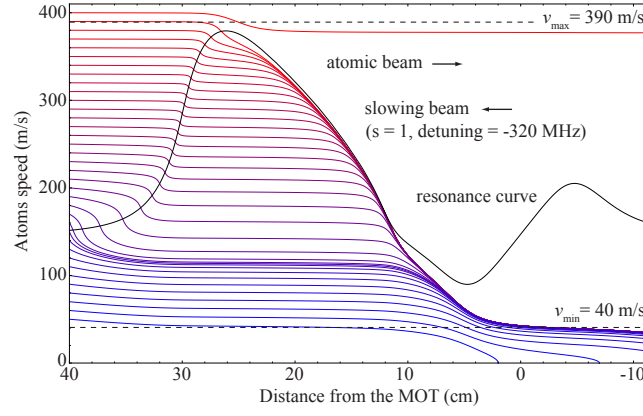


FIG. 4: Simulation of the slowing dynamics with the field profile given by the Zeeman slower coils and the off-axis quadrupole field of the MOT coils.

[24]. With repumpers we measured $N_{st} = 4.5 \times 10^7$ ^{88}Sr atoms, corresponding to an atomic density of $n_0 = 8 \times 10^9 \text{ cm}^{-3}$, $\tau = 282 \text{ ms}$ and $\beta' = 1 \times 10^{-8} \text{ s}^{-1}$, leading to a rate of captured atoms of $\phi_c = N_{st}/\tau + \beta' N_{st}^2 = 9.7 \times 10^7 \text{ s}^{-1}$. Considering that the rate of atoms effused by the oven in the solid angle covered by the Zeeman slowing beam is $6.5 \times 10^8 \text{ s}^{-1}$, about 15 % of the atoms are actually trapped into the blue MOT. This efficiency is mostly determined by the optical pumping into the $4d^1D_2$ state, where atoms can be considered lost from the slowing dynamics since the state lifetime is comparable to the slowing time scale. The probability of an atom of decaying into the ground state after the absorption of n photons is

$$\left(\frac{\Gamma_b}{\Gamma_b + \Gamma_d} \right)^n \simeq \left(1 - \frac{\Gamma_d}{\Gamma_b} \right)^n \simeq \exp \left(-\frac{\Gamma_d}{\Gamma_b} n \right). \quad (1)$$

where $\Gamma_b = 2.0 \times 10^8 \text{ s}^{-1}$ and $\Gamma_d = 3.9 \times 10^3 \text{ s}^{-1}$ are the decay rates of the state 1P_1 into 1S_0 and 1D_2 states, respectively. Therefore the actual fraction of slowed atoms can be estimated through

$$\eta \equiv \int_{v_{\min}}^{v_{\max}} \exp \left(-\frac{\Gamma_d}{\Gamma_b} n(v) \right) f(v) dv \simeq 20 \%, \quad (2)$$

where $v_{\min} = 40 \text{ m/s}$ is the minimum final velocity of atoms at the end of the slowing dynamics, $v_{\max} = 390 \text{ m/s}$ is the maximum atom velocity that can be slowed down (according to the results of numerical simulation shown in Fig. 4), $n(v) = (v - v_{\min})/v_{\text{rec}}$ is the number of photons necessary to reduce the atom velocity from v to v_{\min} , $v_{\text{rec}} = h/\lambda M \simeq 1 \text{ cm/s}$ is the recoil velocity due to the absorption of a photon at 461 nm and $f(v)$ is the velocity distribution in an effusive atomic beam at $T = 380^\circ\text{C}$

$$f(v) = 2 \left(\frac{M}{2k_B T} \right)^2 v^3 \exp \left(-\frac{Mv^2}{2k_B T} \right). \quad (3)$$

Therefore the estimation of the Zeeman slower efficiency $\eta \simeq 20 \%$ given by Eq. 2 is close to the measured value. Additionally the Blue MOT population enhancement factor due to the operation of Zeeman slower can be estimated from the ratio between the actual fraction of slowed atoms η and the fraction of trapped atoms without Zeeman slower

$$\eta / \int_0^{v_c} f(v) dv \simeq 70, \quad (4)$$

which is close to the measured value of ~ 40 .

The final temperature of the blue MOT is minimized by continuously reducing the optical power of the cooling beams from the initial total saturation parameter of $s = 1$ to a final value of $s = 5 \times 10^{-3}$ in 10 ms . This power-reduced phase lasts for 50 ms , leading to a final temperature of the blue MOT of about $\sim 2 \text{ mK}$ measured with absorption imaging (see Fig. 5).

The second laser-cooling stage is performed by using the 1S_0 - 3P_1 intercombination transition at 689 nm (red MOT). The optical beams needed for this phase are superimposed on the blue MOT beams through the three dichroic beam expanders. The $1/e^2$ diameter of the beams for the red MOT is 10 mm and the total intensity incident on the atoms

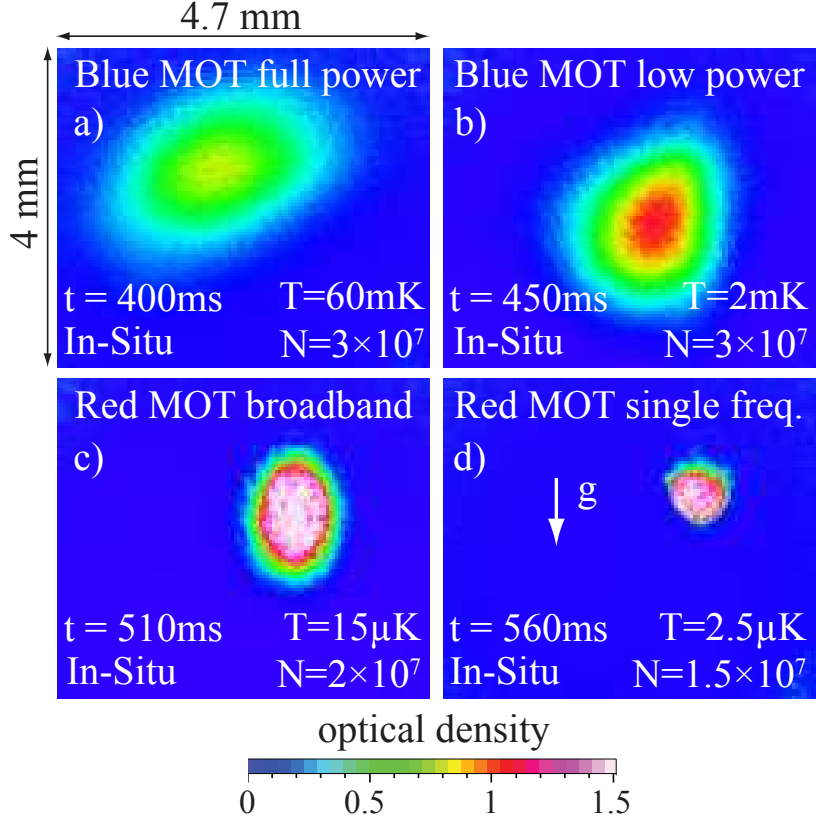


FIG. 5: Absorption imaging *in-situ* of the atomic sample at the relevant phases of the laser cooling sequence lasting a time t , with a constant blue MOT loading time of 400 ms. a) blue MOT full power. b) blue MOT low power. c) red MOT broadband. d) red MOT single frequency.

is 60 mW/cm^2 . The atomic sample at the end of the first cooling stage ($T \sim 2 \text{ mK}$) has a Doppler width of $\sim 2 \text{ MHz}$, too large to be efficiently transferred into the red MOT operating on a 7 kHz natural linewidth transition. For this reason the spectrum of the 689 nm laser is artificially broadened [25, 26]. This is realized by modulating the radio frequency driving of the AOM setting the frequency detuning of the cooling beams. The modulation frequency is 50 kHz , with a span of 4 MHz , leading to an optical spectrum of ~ 80 sidebands, with a saturation parameter of 400 for each one, with the closest to resonance by -300 kHz . This so called red MOT broadband cooling phase lasts for 60 ms and more than 70% of the blue MOT population is transferred into the red MOT. At the beginning of this phase the Zeeman slower field is turned off and the MOT magnetic field gradient is only 20 mT/m in order to have all the atomic velocity classes resonant with the cooling light and it is linearly increased to 70 mT/m in a time interval of 30 ms to compress the atomic sample. With a blue MOT loading time of 400 ms the final population of the broadband red MOT is 2×10^7 atoms, with an atomic density of $1.5 \times 10^{11} \text{ cm}^{-3}$ and a temperature of $\sim 15 \mu\text{K}$.

The second laser-cooling phase is completed by employing a single frequency red MOT, with a detuning of -300 kHz , a constant magnetic field gradient of 20 mT/m and reducing the total intensity of the cooling beams down to $500 \mu\text{W/cm}^2$ in 50 ms . The single frequency red MOT phase produces a sample of 1.5×10^7 atoms, with an atomic density of $2 \times 10^{11} \text{ cm}^{-3}$ and a temperature of $\sim 2.5 \mu\text{K}$. Since the gravity force is comparable to the radiation force of the red MOT beams, the atomic sample sags down from the center of the MOT quadrupole field, assuming an half-disk-like shape with a vertical and horizontal diameter of $500 \mu\text{m}$ [26].

In order to have a long Doppler-free interrogation time of the clock transition, the laser-cooled strontium sample is trapped into a vertical lattice realized by retroreflecting a 290 mW laser beam near the magic wavelength for ^{88}Sr $\lambda_{\text{magic}} = 813.42757(62) \text{ nm}$ [27]. At this wavelength the light shifts of the $^1\text{S}_0$ and $^3\text{P}_0$ level are equal, so that the frequency of the clock transition $^1\text{S}_0 - ^3\text{P}_0$ is not light-shifted by the lattice. The lattice laser output is coupled into a single mode fiber delivering an optical beam with $1/e^2$ diameter of 1.2 mm , which is expanded and focused into the red MOT by a 300 mm focal length lens. The latter is mounted on a 3-axis translation stage with micro-metric actuators, so that the alignment of the beam onto the red MOT can be finely tuned. The resulting beam waist radius on the atomic cloud is $w_0 \sim 40 \mu\text{m}$. After the focus, the divergent lattice beam is then collimated and retroreflected

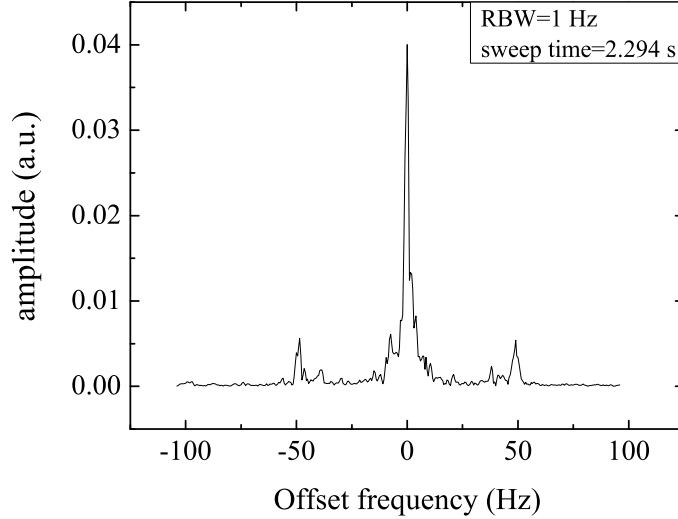


FIG. 6: Beatnote of the transportable laser with a stationary clock laser at 698 nm. The estimated emission linewidth for each laser is 1 Hz.

by means of a dichroic mirror. The latter is employed to couple into the lattice the clock probe beam at $\lambda_c = 698$ nm. The resulting beam diameter of the clock light on the atoms is $74 \mu\text{m}$. Taking into account the power losses due to the telescope, focusing optics and cell windows the estimated lattice trap depth is $U_0 \simeq 76 E_{\text{rec}}$ (corresponding to $\sim 12 \mu\text{K}$, in temperature units), where $E_{\text{rec}} = \hbar^2 k^2 / 2m$ is the photon recoil energy with the wavevector $k = 2\pi / \lambda_{\text{magic}}$ of the lattice light and m the atomic mass of ^{88}Sr . At this depth of the potential the estimated longitudinal trap frequency is $\nu_z = 2E_{\text{rec}} \sqrt{U_0 / E_{\text{rec}}} / \hbar = 60 \text{ kHz}$.

The lattice is continuously operating and at the end of the second laser-cooling stage about 3×10^5 atoms remain trapped, populating ~ 1000 sites, for a total extension of $\sim 400 \mu\text{m}$ corresponding to the vertical size of the red MOT. The $1/e^2$ radius of the atomic cloud trapped in the lattice is measured with absorption imaging to be $\sigma_r = 11 \mu\text{m}$. The longitudinal $1/e^2$ radius of a single site, of the order of $\lambda_L / 2$, cannot be resolved by absorption imaging and is estimated from the size $\sigma_z = \sqrt{\hbar / m \omega_z} \sim 45 \text{ nm}$ of the wave function of atoms populating the ground longitudinal vibrational state (is a good approximation since we have $k_B T / \hbar \nu_z \sim 0.9$). Thus the trapping volume for lattice site is $V_{\text{site}} = (2\pi)^{3/2} \sigma_r^2 \sigma_z \simeq 5 \times 10^{-10} \text{ cm}^3$. In order to keep the shift and broadening effects on the clock transition due to atomic collisions [28], we reduced the number of trapped atoms to below 10^4 (less than 10 atoms per site) by reducing the blue total MOT loading time to 100 ms, leading to a peak atomic density per site below $2 \times 10^{-10} \text{ cm}^{-3}$. The number of atoms is controlled by varying the duration of the blue MOT stage and by finely tuning the position of the gate valve separating the oven from the science region.

The lifetime of atoms trapped into the lattice is measured to be 1.4 s, limited by background gas collisions. Both power and frequency of the lattice laser are not stabilized. The relative RMS power fluctuation is below the 1 % level. The lattice wavelength is tuned near to the magic wavelength of ^{88}Sr [27], monitored by a wave-meter and measured to be stable at $\lambda = 813.4280(1) \text{ nm}$ over a time scale of several hours.

B. Lattice clock spectroscopy

As a first test of the performance of the transportable clock laser after the two-days, 1300 km-long transportation, the laser was compared with a stationary clock laser [29]. Fig. 6 shows the beat note recorded just after re-installation of the clock laser in the lab. The installation process took about one day, mainly do to re-thermalization of the transportable cavity, which was not actively temperature stabilized during transportation. The beat note shows a linewidth of the order of 1 Hz compatible with the laser frequency stability of $2 - 3 \times 10^{-15}$ at 1 s. The comparison with the stationary clock has also been used to estimate the absolute frequency of the transportable clock laser with an uncertainty of less than 1 MHz.

Considering that the single photon ^{88}Sr clock transition $^1\text{S}_0 - ^3\text{P}_0$ is forbidden at any order, the magnetic-field-induced spectroscopy method is used to controllably allow the clock transition, by means of an external magnetic field

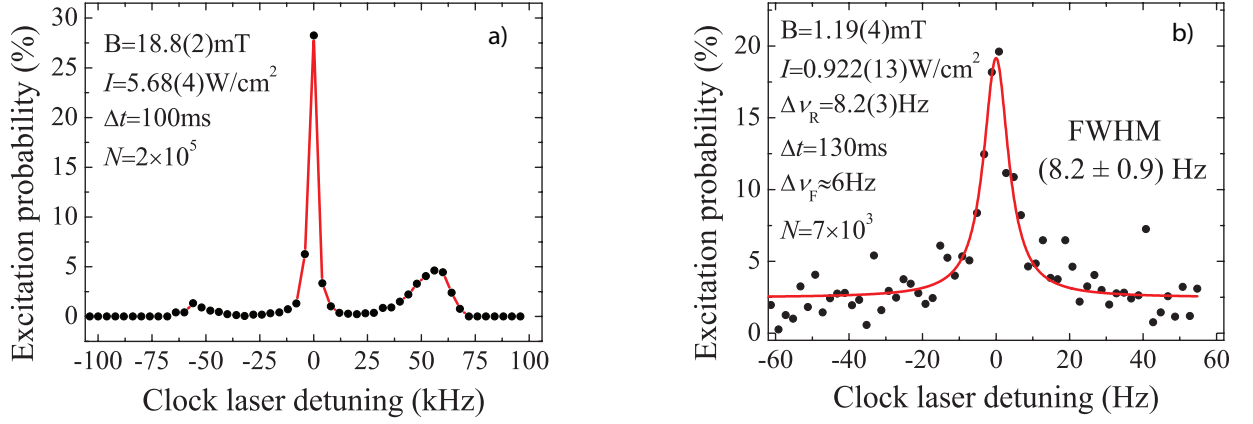


FIG. 7: Spectra of the ^{88}Sr clock transition for different values of the mixing magnetic field $|\mathbf{B}|$, clock probe beam intensity I and excitation pulse length Δt . The frequency axes have arbitrary offsets. The clock resonance is fitted with a Lorentzian function and the obtained FWHM is compared to the Fourier limit linewidth $\Delta\nu_F \simeq 0.8/\Delta t$ and to the Rabi linewidth $\Delta\nu_R = 0.35\sqrt{|\Delta_B\Delta_L|}$, where Δ_B and Δ_L are the second order Zeeman shift and clock probe light shift, respectively (see the text). a) shows a typical search-scan spectrum with the maximum number of atoms loaded into the lattice $N \simeq 2 \times 10^5$. b) is taken with clock interrogation π pulses and a lattice population of $N = 7 \times 10^3$.

coupling the $^3\text{P}_0$ to the $^3\text{P}_1$ state [30]. The search-scan is performed by using a mixing magnetic field of $|\mathbf{B}| = 19 \text{ mT}$ and a clock probe beam intensity of $I = 5.7 \text{ W/cm}^2$, leading to a Rabi frequency of 275 Hz, given by

$$\Omega_R = \alpha\sqrt{I}|\mathbf{B}| \quad (5)$$

where $\alpha(\text{Sr}) = 198 \text{ Hz}/(\text{T}\sqrt{\text{mW/cm}^2})$ [30]. In order to have a high-contrast spectrum the excitation pulse length is $\Delta t = 100 \text{ ms}$, thus overdriving the clock transition having an estimated π pulse duration of $\Delta t_\pi = 1.8 \text{ ms}$. In the search-mode the clock laser frequency is changed by 4 kHz, covering a span of 200 kHz in about 50 s (experiment cycle 1 s). A typical search-mode scan is shown in Fig. 7. The excitation probability is given by the ratio $n(^3\text{P}_0)/[n(^1\text{S}_0) + n(^3\text{P}_0)]$, where $n(^3\text{P}_0)$ and $n(^1\text{S}_0)$ is the atomic population of the $^3\text{P}_0$ and $^1\text{S}_0$ state, respectively. The $^1\text{S}_0$ population is obtained through absorption imaging of the atomic sample after the clock transition interrogation. Atoms in the $^1\text{S}_0$ state are blown away from the lattice by the resonant 461 nm imaging beam. The atoms excited into the $^3\text{P}_0$ level by the clock probe beam are pumped back into the $^1\text{S}_0$ state by means of a 50 ms pulse at 679 nm and 707 nm. The $^1\text{S}_0$ population is then measured through an additional absorption imaging sequence. From the spectra in Fig. 7a, the motional sidebands are measured at $\sim 65 \text{ kHz}$ from the carrier, thus corresponding to a Lamb-Dicke parameter $\eta = \sqrt{\nu_R/\nu_z} \simeq 0.3$, where $\nu_R = h/(2m\lambda^2)$ is the atomic recoil frequency shift associated to the absorption of a photon with $\lambda = 698 \text{ nm}$. The excitation probability in the search-mode scan is only $\sim 30\%$ since the actual clock transition is under-sampled because of the need of covering a large scanning span in reduced time. The excitation pulse duration in this high-resolution mode is chosen to realize an effective π pulse for each configuration of magnetic field and probe intensity. For this purpose the actual atomic Rabi frequency is measured through the observation of the Rabi oscillations (see Fig. 8). On the carrier the excitation probability approaches the 70 % level. We find that the fitted Rabi frequency is about 50 % of the one calculated from Eq. 5, an effect we attribute, together with the reduced excitation probability of 70 %, to the inhomogeneous distribution of the Rabi frequency among the atoms that could be given by a residual spatial inhomogeneity of the clock probe, by a residual misalignment between the probe and lattice axes (estimated to $\sim 1 \text{ mrad}$) and by the thermal transverse atomic motion in the lattice potential [31]. This effect can be significantly reduced by employing a probe beam with larger diameter and a colder atomic sample. By reducing both the mixing magnetic field and the clock probe intensity the low drift rate of the clock laser (few mHz/s) allowed us to reliably measure Rabi oscillations lasting for more than 100 ms and Fourier limited spectra below the 10 Hz FWHM linewidth (see Fig. 8).

A study of the systematics has been carried out and values of estimated shifts on the $^1\text{S}_0$ - $^3\text{P}_0$ clock transition are reported in Table I.

The 2nd order Zeeman and probe Stark shifts have been evaluated by scanning around the clock transition and interleaving measurements with different values of the magnetic field and probe power. As frequency reference we rely on the clock cavity resonance whose typical 1 Hz/s linear drift was compensated to better than 10 mHz/s with a programmable feed-forward AOM driver.

Magnetic field and clock probe power are monitored at 1 % precision level with a Hall probe and a photodiode,

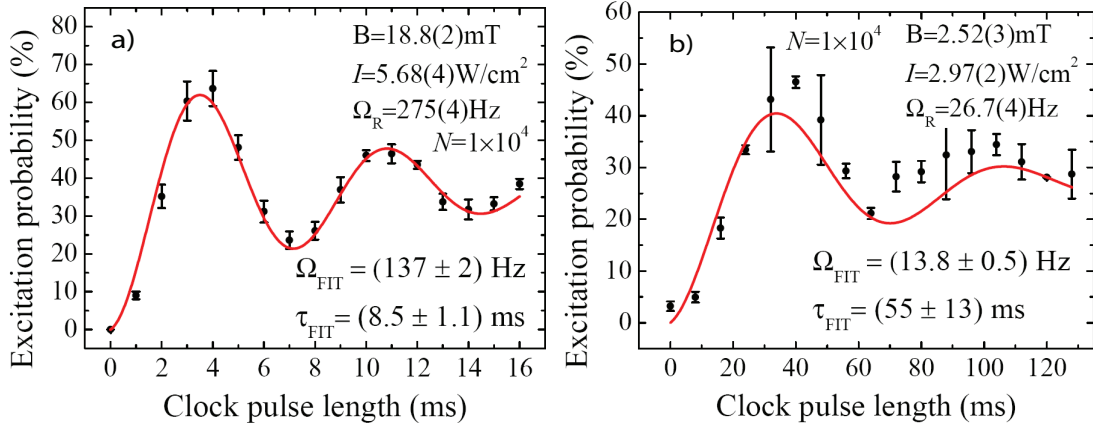


FIG. 8: Measurement of the Rabi oscillations in condition of resonance with the clock transition for different values of the mixing magnetic field and clock probe beam intensity. The data are fitted with the function $a(1 - \cos(2\pi\Omega_{\text{FIT}}\Delta t) \exp(-\Delta t/\tau_{\text{FIT}}))$, where Ω_{FIT} is the actual atomic Rabi frequency and τ_{FIT} gives the decoherence time-scale. The measured atomic Rabi frequency Ω_{FIT} is $\sim 50\%$ of the estimated Rabi frequency Ω_R calculated from the mixing magnetic field and clock laser intensity (see Eq. 5). The corresponding π pulse interrogation length $\Delta t_\pi = 1/2\Omega_{\text{FIT}}$ was employed for the clock spectra b) of Fig. 7.

TABLE I: Systematic frequency shift and uncertainty budget for the ^{88}Sr optical lattice clock as extracted from spectra of the clock transition. The values are reported for the operating conditions of the 8.0(0.1) Hz clock transition linewidth (Fig. 7 b)).

Contributor	Shift (Hz)	Uncertainty (Hz)
2nd order Zeeman	-33.5	2.4
Clock light	-16.6	0.2
Collisions	1.0	0.4
Blackbody radiation	-2.5	0.5
AC Stark (lattice)	-0.7	0.9
Total Uncertainty		2.8

respectively. They are calibrated through the known coefficient β and k [30] by measuring the clock frequency shift as a function of the magnetic field (2.2 – 4.1 mT range, also inverting the direction of the field) and probe intensity (0.9 – 3.2 W/cm² range), as shown in Fig. 9. Values are calculated for the 8.0(0.1) Hz linewidth clock transition (see Table I), obtained with a magnetic field of $|\mathbf{B}| = 1.19(4)$ mT and probe beam intensity of $I = 0.922(13)$ W/cm², corresponding to a second order Zeeman shift and probe AC Stark shift of $\Delta_B = \beta|\mathbf{B}|^2 = -33.5(2.4)$ Hz and $\Delta_L = kI = -16.6(2)$ Hz respectively, where $\beta = -23.3$ Hz/mT² and $k = -18$ Hz/(W/cm²) [30]. The uncertainties on the second order Zeeman shift and probe light shift are given by the quadratic sum of the standard error from the fit and the error associated by the voltage reading on the Hall probe and the photodetector.

The effects of collisions on the ^{88}Sr clock transition have been studied in detail in [28]. In our optimal conditions the number of atoms trapped into the lattice is kept at $7.0(7) \times 10^3$ (~ 7 atoms per site), so that the corresponding peak atomic density per lattice site of $\rho = 1.39(14) \times 10^{10}$ cm⁻³ leads to a collisional shift and broadening of $\rho \times \Delta\nu_\rho = 1.0(4)$ Hz and $\rho \times \gamma_{\text{dep}}/\pi = 1.4(6)$ Hz respectively, with the coefficients $\Delta\nu_\rho = (7.2 \pm 2.0) \times 10^{-11}$ Hz/cm³ and $\gamma_{\text{dep}} = (3.2 \pm 1.0) \times 10^{-10}$ cm³/s [28]. The uncertainties on collisional shift and broadening take into account our experimental 10% fluctuation of the number of atoms shot-to-shot and the uncertainties of the $\Delta\nu_\rho$ and γ_{dep} coefficients and density determination.

During the clock spectroscopy measurement the vacuum chamber temperature is monitored with one thermistor directly attached to the main chamber. No water cooling is employed to cool the MOT coils and after a warm up of about three hours, the temperature of the whole cell stabilizes to 318 K. While a more detailed study of temperature gradients is mandatory for accuracy level below the 10^{-16} level, this lies beyond the scope of the present article. We estimated the blackbody radiation shift to -2.5 Hz with an uncertainty of 0.5 Hz, including the uncertainty due to temperature gradients up to ± 10 K inside the main cell. The AC Stark shift induced by the lattice light has been evaluated considering the effect of the detuning of 0.40 pm with respect to the magic wavelength for ^{88}Sr (with a scalar coefficient 8 Hz/nm/ E_R). Taking also into account the uncertainty in the knowledge of the magic wavelength and the smaller contribution from hyperpolarizability effect [32], the shift amount to 0.3(4) Hz. The amplified spontaneous

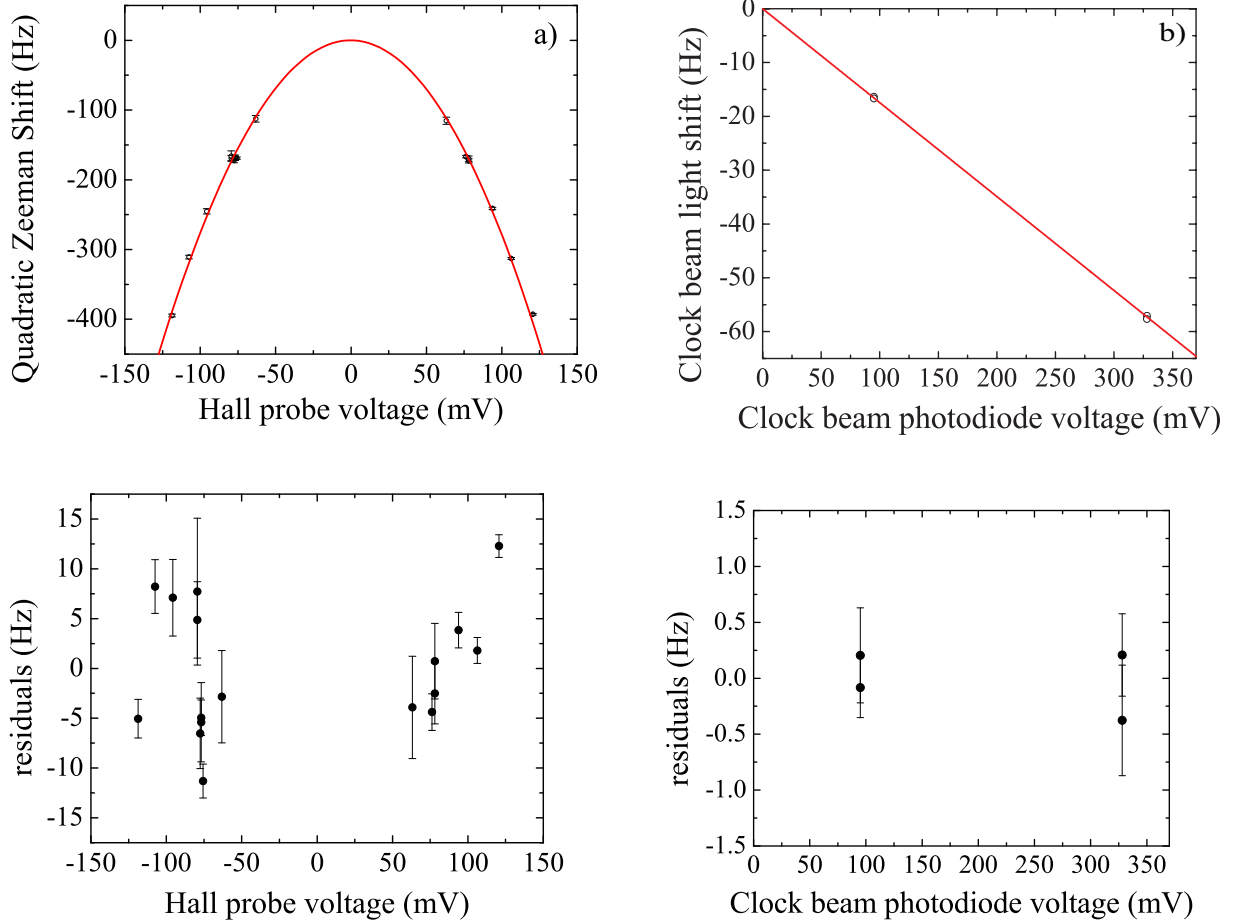


FIG. 9: Systematic shifts of the 1S_0 - 3P_0 clock transition in ^{88}Sr optical lattice clock. a) Measurement of the second order Zeeman shift as a function of the Hall probe voltage. b) Measurement of the probe AC linear Stark shift as a function of the photodiode voltage. The respective curves are used to calibrate the Hall probe and the photodiode to estimate the applied magnetic field \mathbf{B} and the probe light intensity I through the knowledge of the shift coefficients [30]. The two calibration coefficients are $\gamma = 29.0(4)$ mV/mT for the Hall probe and $\eta = 104(1)$ mV/(W cm $^{-2}$) for the photodiode, respectively.

emission (ASE) from the tapered amplifier used for lattice laser is about 40 nm wide and symmetric around the emission wavelength. With a typical ASE intensity 40 dB below the carrier, we estimated an additional shift of $-1.0(5)$ Hz due to this effect. The total value for the AC Stark shift has been evaluated to be $-0.7(9)$ Hz. At 8 Hz clock transition linewidth the achieved total fractional uncertainty is $\sim 7 \times 10^{-15}$, with a transition quality factor of $Q \sim 5 \times 10^{13}$. With a current clock cycle time of $T_c = 1$ s (mainly limited by technical delays in the absorption imaging detection) and an interrogation time $\Delta t = 130$ ms, the stability of the clock is limited at 4×10^{-15} at 1 s by the Dick effect [33]. With minor changes to the detection system a reduction of the clock cycle time to ~ 400 ms can be implemented, maintaining the same number of atoms into the lattice, thus reducing the contribution of the Dick noise below 2×10^{-15} level.

IV. CONCLUSIONS

We presented a compact and transportable optical clock based on strontium atoms. Novel design solutions allowed us also to reduce the volume, weight and power consumption with respect to traditional laser cooling apparatus. As a result the experimental physics package is contained in a volume of less than 2 m 3 and no water cooling is needed to operate the clock. Furthermore, a modular architecture ensured a high degree of operation reliability of the apparatus both in stationary condition and after a transportation of the experimental set up. To ensure high clock frequency

stability, cooling and trapping stages have been optimized to allow high efficiency transfer among different cooling and trapping stages, thus allowing for faster clock cycle time with high duty cycle. Spectroscopy on $^1\text{S}_0$ - $^3\text{P}_0$ clock transition on bosonic ^{88}Sr isotopes has been demonstrated with an 8 Hz resolution. Eventually, an evaluation of the main systematic frequency shifts on the clock transition has been done and the fractional uncertainty of the clock is 7×10^{-15} .

The authors acknowledge financial support from ESA and the European Union Seventh Framework Programme (FP7/2007-2013 grant agreement 263500, project “Space Optical Clocks”) and the European Metrology Research Programme (EMRP) under IND14. The EMRP is jointly funded by the EMRP participating countries within EURAMET and the European Union. We also acknowledge support by the DFG RTG 1729 “Fundamentals and applications of ultra-cold matter”. We thank D. V. Sutyurin for useful discussions.

-
- [1] N. Poli, C. W. Oates, P. Gill, and G. M. Tino. Optical atomic clocks. *Rivista del Nuovo Cimento*, 36:555–624, 2013.
 - [2] B. J. Bloom, T. L. Nicholson, J. R. Williams, S. L. Campbell, M. Bishof, X. Zhang, W. Zhang, S. L. Bromley, and J. Ye. An optical lattice clock with accuracy and stability at the 10^{-18} level. *Nature*, 506:71–75, 2014.
 - [3] C. W. Chou, D. B. Hume, J. C. J. Koelemeij, D. J. Wineland, and T. Rosenband. Frequency comparison of two high-accuracy Al^+ optical clocks. *Phys. Rev. Lett.*, 104(7):070802, 2010.
 - [4] N. Hinkley, J. A. Sherman, N. B. Phillips, M. Schioppo, N. D. Lemke, K. Beloy, M. Pizzocaro, C. W. Oates, and A. D. Ludlow. An atomic clock with 10^{-18} instability. *Science*, 341(6151):1215–1218, 2013.
 - [5] S. Schiller, G. M. Tino, P. Gill, C. Salomon, U. Sterr, E. Peik, A. Nevsky, A. Goerlitz, D. Svehla, G. Ferrari, N. Poli, L. Lusanna, H. Klein, H. Margolis, P. Lemonde, P. Laurent, G. Santarelli, A. Clairon, W. Ertmer, E. Rasel, J. Mueller, L. Iorio, C. Laemmerzahl, H. Dittus, E. Gill, M. Rothacher, F. Flechner, U. Schreiber, V. Flambaum, Wei-Tou Ni, Liang Liu, Xuzong Chen, Jingbiao Chen, Kelin Gao, L. Cacciapuoti, R. Holzwarth, M. P. Hess, and W. Schaefer. Einstein gravity explorer-a medium-class fundamental physics mission. *Exp. Astron.*, 23(2):573–610, 2009.
 - [6] P. Wolf, Ch. J. Borde, A. Clairon, L. Duchayne, A. Landragin, P. Lemonde, G. Santarelli, W. Ertmer, E. Rasel, F. S. Cataliotti, M. Inguscio, G. M. Tino, P. Gill, H. Klein, S. Reynaud, C. Salomon, E. Peik, O. Bertolami, P. Gill, J. Paramos, C. Jentsch, U. Johann, A. Rathke, P. Bouyer, L. Cacciapuoti, D. Izzo, P. De Natale, B. Christophe, P. Touboul, S. G. Turyshev, J. Anderson, M. E. Tobar, F. Schmidt-Kaler, J. Vigue, A. A. Madej, L. Marmet, M. C. Angonin, P. Delva, P. Tournenc, G. Metris, H. Mueller, R. Walsworth, Z. H. Lu, L. J. Wang, K. Bongs, A. Toncelli, M. Tonelli, H. Dittus, C. Laemmerzahl, G. Galzerano, P. Laporta, J. Laskar, A. Fienga, F. Roques, and K. Sengstock. Quantum physics exploring gravity in the outer solar system: the sagas project. *Exp. Astron.*, 23(2):651–687, 2009.
 - [7] C. W. Chou, D. B. Hume, T. Rosenband, and D. J. Wineland. Optical clocks and relativity. *Science*, 329(5999):1630–3, 2010.
 - [8] T. M. Fortier, M. S. Kirchner, F. Quinlan, J. Taylor, J. C. Bergquist, T. Rosenband, N. Lemke, A. Ludlow, Y. Jiang, C. W. Oates, and S. A. Diddams. Generation of ultrastable microwaves via optical frequency division. 5(7):425–429, 2011.
 - [9] A. E. Rogers, R. J. Cappallo, H. F. Hinteregger, J. I. Levine, E. F. Nesman, J. C. Webber, A. R. Whitney, T. A. Clark, C. Ma, J. Ryan, B. E. Corey, C. C. Counselman, T. A. Herring, I I Shapiro, C. A. Knight, D. B. Shaffer, N. R. Vandenberg, R. Lacasse, R. Mauzy, B. Rayhrer, B. R. Schupler, and J. C. Pigg. Very-long-baseline radio interferometry: The mark III system for geodesy, astrometry, and aperture synthesis. *Science*, 219(4580):51–4, 1983.
 - [10] D. R. Leibrandt, M. J. Thorpe, J. C. Bergquist, and T. Rosenband. Field-test of a robust, portable, frequency-stable laser. *Opt. Expr.*, 19(11):10278–10286, 2011.
 - [11] K. Predehl, G. Grosche, S. M. F. Raupach, S. Droste, O. Terra, J. Alnis, Th. Legero, T. W. Hänsch, Th. Udem, R. Holzwarth, and H. Schnatz. A 920-kilometer optical fiber link for frequency metrology at the 19th decimal place. *Science*, 336(6080):441–4, 2012.
 - [12] P. A. Williams, W. C. Swann, and N. R. Newbury. High-stability transfer of an optical frequency over long fiber-optic links. *J. Opt. Soc. Am. B-Opt. Phys.*, 25(8):1284–1293, 2008.
 - [13] D. Calonico, E. K. Bertacco, C. E. Calosso, C. Clivati, G. A. Costanzo, A. Godone, M. Frittelli, A. Mura, N. Poli, D. V. Sutyurin, G. M. Tino, M. Zucco, and F. Levi. High accuracy coherent optical frequency transfer over a doubled 642 km fiber link *arXiv:1404.0395*, in publication on *Appl. Phys. B* DOI: 10.1007/s00340-014-5917-8, 2014.
 - [14] S. Bize, P. Laurent, M. Abgrall, H. Marion, I. Maksimovic, L. Cacciapuoti, J. Grunert, C. Vian, F.P. dos Santos, P. Rosenbusch, P. Lemonde, G. Santarelli, P. Wolf, A. Clairon, A. Luiten, M. Tobar, and C. Salomon. Cold atom clocks and applications. *J. Phys. B-At. Mol. Opt. Phys.*, 38(9, SI):S449–S468, 2005.
 - [15] N. Poli, R. E. Drullinger, M. G. Tarallo, G. M. Tino, and M. Prevedelli. Strontium optical lattice clock with all semiconductor sources. In *Proceedings of the 2007 IEEE International Frequency Control Symposium-jointly with the 21st European Frequency and Time Forum, Vols 1-4*, pages 655–658, 2007.
 - [16] N. Poli, M. G. Tarallo, M. Schioppo, C. W. Oates, and G. M. Tino. A simplified optical lattice clock. *Applied Physics B*, 97:27, 2009.
 - [17] H. Katori, K. Hashiguchi, E. Yu. Il’ina, and V. D. Ovsiannikov. Magic wavelength to make optical lattice clocks insensitive to atomic motion. *Phys. Rev. Lett.*, 103:153004, 2009.
 - [18] M. Schioppo. *Development of a Transportable Strontium Optical Clock*. PhD thesis, Dipartimento di Fisica e Astronomia,

Università di Firenze, Firenze, December 2010.

- [19] M. Schioppo, N. Poli, M. Prevedelli, S. Falke, Ch. Lisdat, U. Sterr, and G. M. Tino. A compact and efficient strontium oven for laser-cooling experiments. *Rev. Sci. Instrum.*, 83(10, 1), 2012.
- [20] X. Baillard, A. Gauguier, S. Bize, P. Lemonde, Ph. Laurent, A. Clairon, and P. Rosenbusch. Interference-filter-stabilized external-cavity diode lasers. *Opt. Commun.*, 266(2):609–613, 2006.
- [21] S. Falke, M. Misera, U. Sterr, C. Lisdat. Delivering pulsed and phase stable light to atoms of an optical clock. *Applied Physics B*, 107(2):301–311, 2012.
- [22] S. Vogt, C. Lisdat, T. Legero, U. Sterr, I. Ernsting, A. Nevsky, and S. Schiller. Demonstration of a transportable 1 Hz-linewidth laser. *Appl. Phys. B-Lasers Opt.*, 104(4):741–745, 2011.
- [23] X. Xu, T. H. Loftus, J. L. Hall, A. Gallagher, and J. Ye. Cooling and trapping of atomic strontium. *J. Opt. Soc. Am. B*, 20(5):968–976, 2003.
- [24] T. P. Dinneen, K. R. Vogel, E. Arimondo, J. L. Hall, and A. Gallagher. Cold collisions of Sr^*-Sr in a magneto-optical trap. *Phys. Rev. A*, 59:1216, 1999.
- [25] H. Katori, T. Ido, Y. Isoya, and M. Kuwata-Gonokami. Magneto-optical trapping and cooling of strontium atoms down to the photon recoil temperature. *Phys. Rev. Lett.*, 82:1116, 1999.
- [26] T. H. Loftus, T. Ido, M. M. Boyd, A. D. Ludlow, and J. Ye. Narrow line cooling and momentum-space crystals. *Physical Review A*, 70:063413, 2004.
- [27] T. Akatsuka, M. Takamoto, and H. Katori. Three-dimensional optical lattice clock with bosonic $\text{Sr}88$ atoms. *Phys. Rev. A*, 81:023402, 2010.
- [28] Ch. Lisdat, J. S. R. Vellore Winfred, T. Middelmann, F. Riehle, and U. Sterr. Collisional losses, decoherence, and frequency shifts in optical lattice clocks with bosons. *Phys. Rev. Lett.*, 103(9), 2009.
- [29] M. G. Tarallo, N. Poli, M. Schioppo, D. Sutyran, and G. M. Tino. A high-stability semiconductor laser system for a $\text{Sr}-88$ -based optical lattice clock. *Appl. Phys. B-Lasers Opt.*, 103(1):17–25, 2011.
- [30] A. V. Taichenachev, V. I. Yudin, C. W. Oates, C. W. Hoyt, Z. W. Barber, and L. Hollberg. Magnetic field-induced spectroscopy of forbidden optical transitions with application to lattice-based optical atomic clocks. *Phys. Rev. Lett.*, 96:083001, 2006.
- [31] S. Blatt, J. W. Thomsen, G. K. Campbell, A. D. Ludlow, M. D. Swallows, M. J. Martin, M. M. Boyd, and J. Ye. Rabi spectroscopy and excitation inhomogeneity in a one-dimensional optical lattice clock. *Phys. Rev. A*, 80:052703, 2009.
- [32] A. Brusch, R. Le Targat, X. Baillard, M. Fouché, and P. Lemonde. Hyperpolarizability effects in a Sr optical lattice clock. *Phys. Rev. Lett.*, 96:103003, 2006.
- [33] A. Quessada, R. P. Kovacich, I. Courtillot, A. Clairon, G. Santarelli, and P. Lemonde. The Dick effect for an optical frequency standard. *J. Opt. B: Quantum Semiclass. Opt.*, 5:S150, 2003.